NPL
National Physical Laboratory

Report

NPL REPORT IR 12

Photon Doses in NPL Standard Radionuclide Neutron Fields

C.J. McKay, P. Burgess,
N.P. Hawkes, M. Kelly,
G.C. Taylor, and
D.J. Thomas.

NOT RESTRICTED

January 2009

National Physical Laboratory | Hampton Road | Teddington | Middlesex | United Kingdom | TW11 0LW
Switchboard 020 8977 3222 | **NPL Helpline** 020 8943 6880 | **Fax** 020 8614 0446 | **www.npl.co.uk**

Department for **Innovation, Universities** & **Skills**

NPL Report IR 12

January 2009

NATIONAL PHYSICAL LABORATORY

Photon Doses in NPL Standard Radionuclide Neutron Fields

by

C.J. McKay, P. Burgess, N.P. Hawkes, M. Kelly, G.C. Taylor, and D.J. Thomas.

Quality of Life Division

ABSTRACT

The photon dose rates from a range of radionuclide neutron sources have been measured using halogen-quenched Geiger-Müller detectors and EPD MkII and EPD-N2 electronic personal dosemeters. The photon spectrum from each source was calculated from available literature, corrected for self-attenuation within the sources, and used to calculate the Geiger-Müller detector response for each source. EPD and EPD-N2 photon dose measurements on-phantom agreed well with the Geiger-Müller detector measurements.

ISSN 1754-2952

National Physical Laboratory
Hampton Road, Teddington, Middlesex, TW11 0LW

Approved on behalf of the Managing Director, NPL by Bajram Zeqiri,
Knowledge Leader, Acoustics & Ionising Radiation Team,
authorised by Susan Evans, Director, Quality of Life Division

Contents

Sections **Page**

Figures

Tables

1 INTRODUCTION

The aim of this work was to add to the National Physical Laboratory's measurement capability by characterising and measuring the photon dose rates in its standard radionuclide neutron fields. This will expand NPL's ability to calibrate and perform radiological type tests on radiometric instruments sensitive to both photons and neutrons.

1.1 Mixed fields

Neutron field, by the nature of their generation and interaction mechanisms, cannot exist in isolation. An accompanying photon field will always be present. These photons originate from both the neutron generating reactions and secondary neutron interactions in the surrounding environment. Thus it is more accurate to view neutron fields as a component of a "mixed field" of both photons and neutrons.

With increasing technological development in the field of radiation dosimetry, the number of instruments that claim to measure both photon and neutron dose is increasing. The calibration and type testing of these instruments presents a challenge as the neutron-sensitive element may have a sensitivity to photons, and vice versa. To measure the response of such devices, the photon and neutron components of the mixed field must be accurately known.

At NPL routine calibrations with sources are performed using the ISO standard ^{241}Am-Be(α,n) or ^{252}Cf(spontaneous fission) sources [1]. Other sources available for performing calibrations are: ^{241}Am-F, ^{241}Am-Li, ^{241}Am-B, and D_2O moderated ^{252}Cf. (The latter two are also ISO recommended sources, although they are seldom used for routine calibrations at NPL.) The neutron emission of these sources is already well known and is regularly checked. However, all of these sources produce significant photon radiation as a result of their neutron generation mechanisms and associated secondary reactions, hence measurement of the photon dose associated with these sources is important.

1.2 Previous measurements

Previous measurements of radionuclide neutron sources have been reported by several authors [2,3,4,5]. However, due to the complexity of radionuclide neutron sources, variations between individual sources are inevitable; and to gain an accurate knowledge of the photon dose rate from a specific source it is important that the photon dose rate from that source is measured. There may also be questions about the validity of the approaches used in earlier measurements.

Previous measurements of the photon dose rates in a variety of radionuclide fields were attempted at NPL using Geiger-Müller detectors; however, unacceptable inconsistencies in the results were observed; and the measurements needed to be reinvestigated.

2 MATERIALS AND METHODS

2.1 Construction of Geiger detectors

Energy-compensated halogen-quenched Geiger-Müller tubes are largely insensitive to fast neutrons, simple to use, and have a relatively flat response with photon energy, which makes them one of the preferred detectors for measuring the photon dose component of a mixed field [6]. Additionally, the useful energy range, from 0.03 to 6 MeV, covers the full range of expected photon energies.

Four halogen-quenched Geiger-Müller tubes of different designs, each with an energy compensation filter, were used for these measurements. The detectors used were: an MX164A, an MX164B, a ZP1100 and an MX163. Their details are given in the manufacturer's data sheets [7,8]. The base detectors used are the Mullard (now Centronic) ZP1320 for the MX164s, the ZP1310 for the ZP1100 and the ZP1300 for the MX163. Details of their construction and of the energy compensation filters are presented in Figure 1. Note that the energy compensation filters used are fairly primitive and more modern designs have better energy dependence and polar responses.

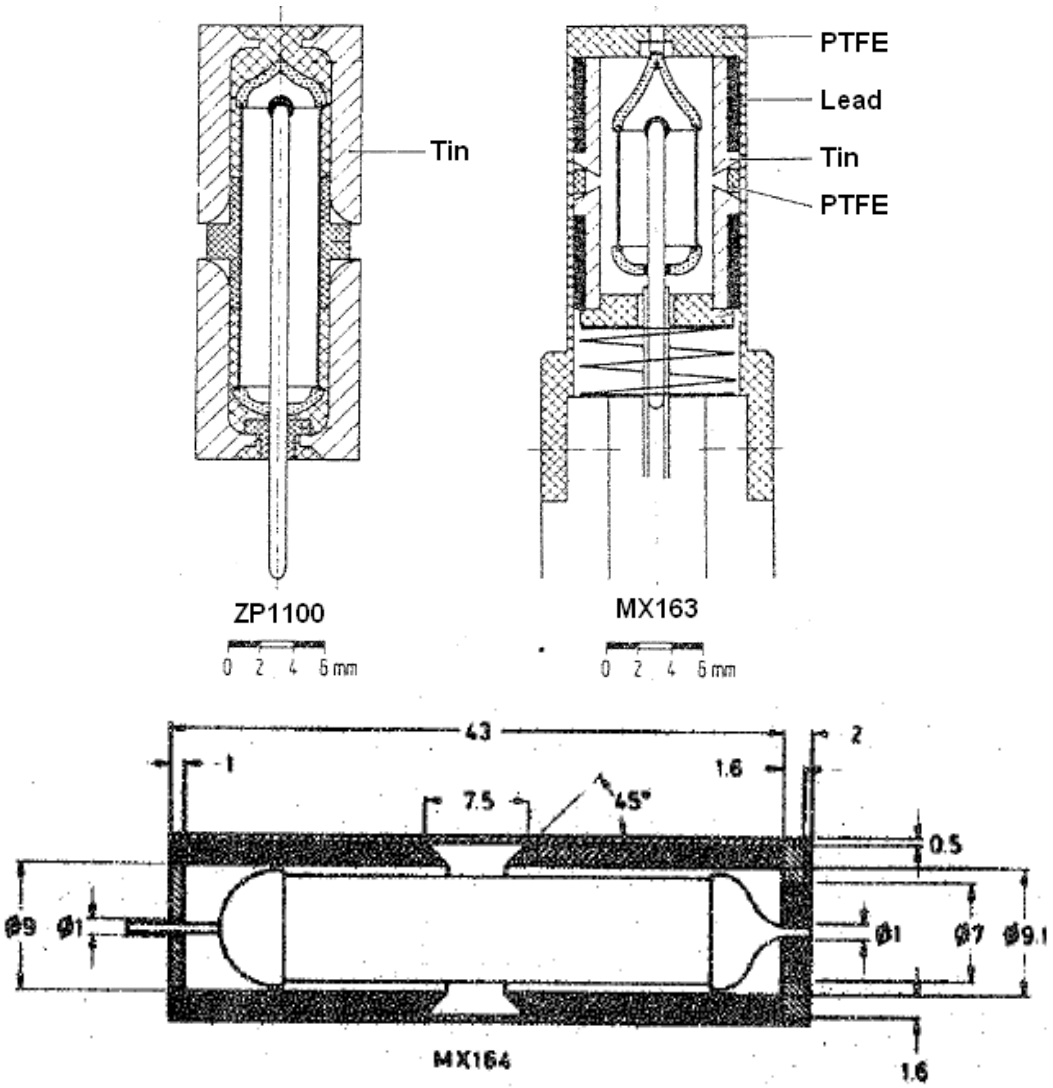

Figure 1. Schematic diagrams of ZP1100 (top left), MX163 (top right), and MX164 detectors (bottom).

The two MX164 devices are very similar except that the Perspex® (PMMA) used in the MX164A is replaced by PTFE in the MX164B model. All four detectors were supplied by AEE Winfrith. The ZP1100 has an integral energy compensation filter that conforms to the original Mullard design. The remaining three detectors are surrounded by an additional energy compensation filter, designed by AEE Winfrith.

2.2 Neutron source construction

The neutron sources studied in this work are listed in Table 1. Knowledge of the photon spectrum from each source is required in order to calculate each Geiger-Müller detector's effective response. In order to determine the photon spectrum seen by the detector as accurately as possible, the effect of self-attenuation by the source and its encapsulation must be considered.

To this end the following simple models of the source capsules, in conjunction with the estimated emission spectra (described in Section 2.3) were used to model the realistic photon spectra at the measurement point. Attenuation corrections were calculated for a distance of 75 cm in air using MicroShield 7.00 [9]. This software uses a simplified deterministic approach, but is sufficient for the present purpose. It only considers attenuating material along a direct path between the emission point and the dose point. As a result the models described below, and illustrated in Figures 2 to 4, only consider attenuating material in the same plane as the detector. The attenuation in the D_2O moderated ^{252}Cf source required more rigorous modelling and was calculated using the Monte Carlo code MCNP.

Table 1. Radionuclide neutron sources used, and their activities on 30/04/2007

Source type	Source reference	Original activity or mass	Mean neutron energy (MeV)[a]	Free field fluence rate at 75cm (cm^{-2} s^{-1})[b]	Mechanism	Capsule construction[c]
^{241}Am-Be	1999NE	555 GBq (15 Ci)	4.16	474	(α, n)	X14 and X14 + 2 mm lead
^{241}Am-B	7584B	37 GBq (1 Ci)	2.72	6.30	(α, n)	X3
^{241}Am-F	7583F	37 GBq (1 Ci)	1.47[d]	1.93	(α, n)	X3
^{241}Am-Li	3250Li	185 GBq (5 Ci)	0.48[e]	3.09	(α, n)	X14 and X14 + 2 mm lead
^{252}Cf	4774 NC	1.7 mg	2.13	93.8	Fission	X35
D_2O mod ^{252}Cf	4774 NC	1.7 mg	0.54	82.2[f]	Fission	X35 in D_2O moderating sphere

a Unless otherwise stated mean neutron energies are taken from ISO 8529-1 [1]
b Free field fluence rate calculated from decay-corrected NPL source emission rate measurements, typical uncertainty is 1%
c The 'X' nomenclature, i.e. X3, X14, etc., was that used by The Radiochemical Centre, Amersham. This has been continued by the current manufacturer QSA Global
d Value is the mean of measurements by Owen *et al*. [10], and by Tagziria [11]
e Value measured by Tagziria *et al*. [12]
f For a D_2O moderated ^{252}Cf. source 11.5% of the neutron fluence is moderated below the cadmium cut-off and captured in cadmium shell [1]

2.2.1 X14 capsule construction (^{241}Am-Be and ^{241}Am-Li)

The ^{241}Am-Be and ^{241}Am-Li sources are encapsulated in X14 type capsules. The active material is a mixture of $^{241}AmO_2$ and beryllium or $^{241}AmO_2$ and lithium hydride. It occupies a

volume of 25.2ø × 46 mm inside the capsule which has outer dimensions of 30ø × 60 mm. The active volume is encapsulated in 2.4 mm thick steel, which for modelling of the photon attenuation, was assumed to be 100% iron. Photon attenuation is primarily due to interaction with the atomic electrons and the exact composition of the capsule is thus unimportant.

For measurements with sources surrounded by lead, the model was altered to include a 2 mm thick lead cylinder with an outer diameter of 74 mm coaxial with the source. Both the bare and lead filtered source attenuation models are shown in Figure 2.

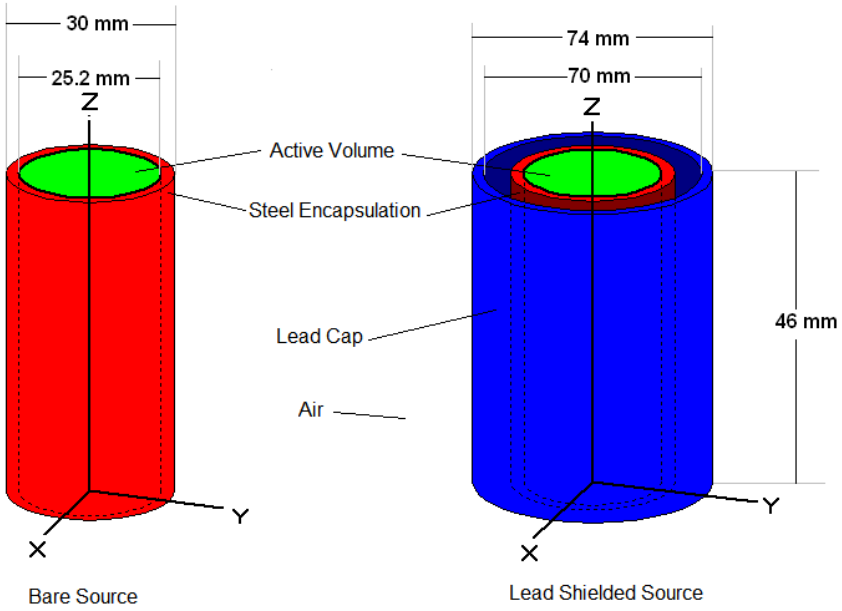

Figure 2. Bare and lead filtered X14 capsule. Note that the height refers to the volume of the active material not the X14 capsule.

2.2.2 X3 capsule construction (^{241}Am-B and ^{241}Am-F)

The ^{241}Am-B and ^{241}Am-F sources are encapsulated in an X3 type capsule, shown in Figure 3. Its construction is similar to the X14, but has an outer diameter of 22.4 mm and a height of 31 mm. The active material is in the form of a mixture of $^{241}AmO_2$ and boron or calcium fluoride. The active material is cylindrical with dimensions 17.5ø × 18.5 mm and is encapsulated in 2.4 mm of steel, which for modelling purposes was assumed to be iron.

2.2.3 X35 capsule construction (^{252}Cf)

The ^{252}Cf source was encapsulated within a modified type X35 capsule. The californium was assumed, for simplicity of modelling, to be embedded in a 10 mm long metal wire at the centre of the capsule and to be surrounded by a 0.65 mm steel wall. For attenuation modelling purposes both the source wire and the steel wall were assumed to be 100% iron. The model used for attenuation correction is shown in Figure 4.

The D_2O moderated ^{252}Cf source is described in detail by Schwartz *et al.*[13]. The previously described ^{252}Cf source is surrounded by a 15 cm radius sphere of D_2O. A 1 mm thick steel shell and a 1 mm thick cadmium shell surrounded this. The photon attenuation model assumed the D_2O was normal water and the steel was 100% iron.

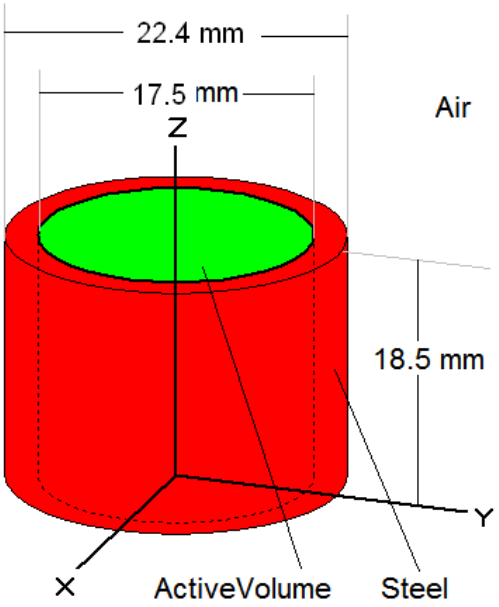

Figure 3. Diagram of X3 capsule model

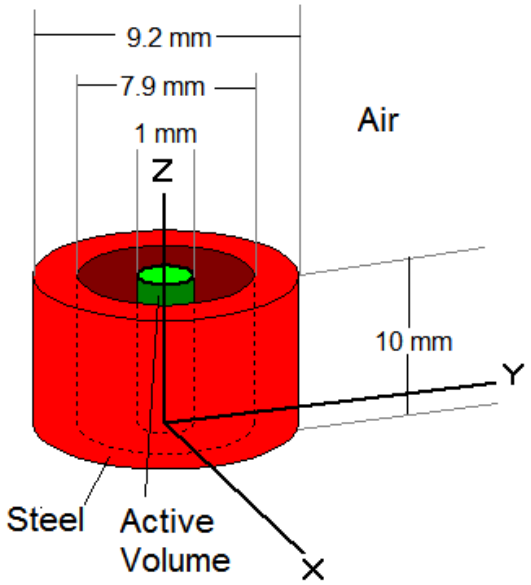

Figure 4. Diagram of X35 capsule model

2.3 Source photon spectra

The photon spectrum at a distance from a radionuclide neutron source is a mixture of the photons emitted directly from the radionuclide and photons from secondary reactions by the emitted radiation. Secondary radiation originates both from reactions in the source itself and from room return, primarily as a result of neutron interactions in the walls. However, measurements of the neutron sources were performed in NPL's low scatter facility and it can be assumed that all the photon radiation measured originates in the source.

2.3.1 Photon spectra of ^{241}Am(α,n) sources

The primary photon component of all the ^{241}Am(α,n) sources originates from excited states in ^{237}Np following alpha decay of the ^{241}Am. Using the ENSDF database [14] in conjunction with available literature characterising the ^{241}Am(α,n) sources allowed the absolute photon emission spectra to be estimated. Attenuation corrections were performed using the source models described in Section 2.2 and the resulting photon spectra are listed and plotted in Appendix A. For all these spectra the effects of Doppler broadening have not been considered and all photon components are assumed to consist of single discrete energies. This approximation has negligible effect on the final results.

For all the ^{241}Am(α,n) sources the ^{241}Am emission spectrum dominates the relative photon fluence spectrum. The contribution from secondary reactions is only significant when the source is behind a lead filter. The ^{241}Am photon spectrum is dominated by the 59.5 keV gamma decay. However, there is a low but non-negligible probability of the emission of higher energy photons, the strongest of which are the 368 keV, 619 keV and 662 keV gamma decays. For a bare source their contribution is small, but their increased penetrating power makes them a significant part of the lead filtered source spectra.

For the ^{241}Am-Be source (ID number 1999NE) the only significant secondary photon emission is from the ^{9}Be(α,n)^{12}C reaction, which results in a roughly 60% probability of 4.439 MeV photon emission [15]. Excited states in ^{9}Be from (α,α') reactions, decay almost

entirely via neutron emission with only a small probability of gamma decay [14]. When a 2 mm lead filter is used the strongest photon component is the 4.439 MeV gamma ray, which then makes up 22% of the total photon fluence. The remainder are other high-energy gamma rays resulting from ^{241}Am decay.

The ^{241}Am-B source has been observed to have a contribution from only three secondary reactions [16]. The $^{11}B(\alpha,n_1)^{14}N$ reaction to the first excited state results in the emission of 2.31 MeV gamma rays, whilst the $^{10}B(\alpha,p\gamma)^{13}C$ reaction results in the emission of 3.68 MeV and 3.85 MeV gamma rays. The majority of the neutrons derive from reactions in ^{11}B. A calculation of the relative intensities of the $^{11}B(\alpha,n_x)^{14}N$ branches, from an integration of the evaluated cross-sections [17] divided by the stopping power for alpha particles in the source medium, enabled the ratio of the $^{11}B(\alpha,n_1)^{14}N$ branch to the sum of all the neutron producing branches to be determined, and hence the 2.31 MeV gamma to neutron ratio. The corresponding ratios for the other two gamma rays were determined from the spectral measurements of Lees and Lindley[16]. From this information the contribution of these components relative to the ^{241}Am gamma rays was calculated. Lees and Lindley also reported a small degree of beryllium contamination, resulting in the observation of a 4.439 MeV gamma ray. Nevertheless it has been shown that for a bare source the contribution from these secondary reactions is small.

Unlike the previously described sources the ^{241}Am-F source has many photon components in addition to the ^{241}Am gamma rays. Whilst it is clear these components exist, estimating their contribution is beyond the simple literature review conducted here. What is clear from a cursory examination of the appropriate neutron production cross-sections is that their contribution to the spectrum of a bare source is negligible. As a result it has been assumed that the photon spectrum is that for ^{241}Am. This assumption is not valid if the source is surrounded by a lead filter and in this case it is recommended that a direct spectroscopic measurement of the source be performed.

The ^{241}Am-Li source by contrast has a simple spectrum, with only one photon component in addition to the ^{241}Am decay spectrum [16]. This is a 0.478 MeV gamma ray, resulting from the $^{7}Li(\alpha,\alpha'\gamma)^{7}Li$ reaction. The ^{241}Am-Li photon emission spectrum, after attenuation with a lead filter, is shown in Appendix A. With the filter in place the spectrum is dominated by the 0.478 MeV gamma ray.

2.3.2 Photon spectrum of a ^{252}Cf source

^{252}Cf has a 96.9% probability of undergoing alpha decay to ^{248}Cm and a 3.1% probability of undergoing spontaneous fission. However, the low photon emission probability and the low energy of the resulting photons means that the photon dose rate following alpha decay is small in comparison to the photon dose rate as a result of spontaneous fission. The photon spectrum resulting from fission is a continuum rather than the discrete energies generated by the other sources. The binned ^{252}Cf prompt and delayed photon spectrum detailed in ICRU 26 [6] was interpolated to provide a finely binned spectrum at intermediate energies. This shows that the average photon energy is ~0.75 MeV. The photon spectrum of the ^{252}Cf source is shown graphically and tabulated in Appendix B.

Defining the photon spectrum from the ^{252}Cf source is made more difficult by the presence of a component from long-lived daughters and from fission products, which increases with the age of the source. The NPL ^{252}Cf source used was 22 years old and no information could be found on the photon spectrum of a source of this age.

However, examination of the ^{252}Cf fission fragment yields [18] and the decay chains of the produced nuclides indicates that the only significant build-up is that of ^{137}Cs. This has a 30 year half-life and emits a 662 keV gamma ray following β decay. The similarity of the 662 keV gamma ray to the average photon energy given by ICRU 26 for ^{252}Cf photons, indicates that the detector sensitivity will not be significantly altered by the presence of ^{137}Cs. As a result a lack of knowledge about the ^{137}Cs contribution will not have a significant effect on the detector response or dose conversion factors.

2.3.3 D_2O moderated ^{252}Cf photon spectrum

The photon attenuation direct from the source was modelled using MCNP because of the good geometry capabilities of this code. The steel shell was assumed to be iron and the D_2O assumed to be ordinary water.

The radiative capture within the source was also modelled using MCNP and photon emission following thermal neutron capture by the < 1% H_2O content of the D_2O was shown to be negligible. Cross section data for photon production following neutron capture in cadmium were not present in the MCNP data libraries. Consequently, the photon contribution from the cadmium was calculated simply by multiplying the number of neutrons captured by the cadmium by published capture-gamma intensities for each energy of gamma. Previous measurements by Schwartz *et al.*[13] showed the capture percentage to be 11.5% of the total neutron fluence for a ^{252}Cf source. The capture gamma ray emission rate and attenuated spectrum were calculated using the IAEA PGAA database [19]. The spectrum is shown in Appendix B. The cadmium capture peaks can be clearly seen, however, the contribution from cadmium capture was shown to be less than 1% of the total photon fluence.

2.4 Neutron response of Geiger tubes

The mixed field reading, R_u, (expressed in terms of counts) of a detector such as a Geiger-Müller tube that is sensitive to both photons and neutrons can be expressed as:

$$R_u = b(k_u K_n + h_u K_\gamma) \tag{1}$$

where:

b is the reading per unit kerma or dose for the gamma rays used for calibration [Gy^{-1}]

k_u is the ratio of the detector's sensitivity to neutrons to its sensitivity to the gamma rays used for calibration

K_n is the neutron kerma or dose in the mixed field [Gy]

h_u is the ratio of the detector's sensitivity to photons in the mixed field to its sensitivity to the gamma rays used for calibration - see section 3.1

K_γ is the photon kerma or dose in the mixed field [Gy]

The sensitivity, b, is determined as the counts per unit value of the calibration quantity, which is chosen to be the same as the desired quantities K_n and K_γ. This could be, for example, kerma in air; however, published values of the neutron response k_u are given in terms of absorbed dose in tissue. A review of the literature on k_u values of the types of Geiger-Müller detectors used in this study was conducted and the values, plotted over a range of energies, are shown in Figures 5, 6, and 7.

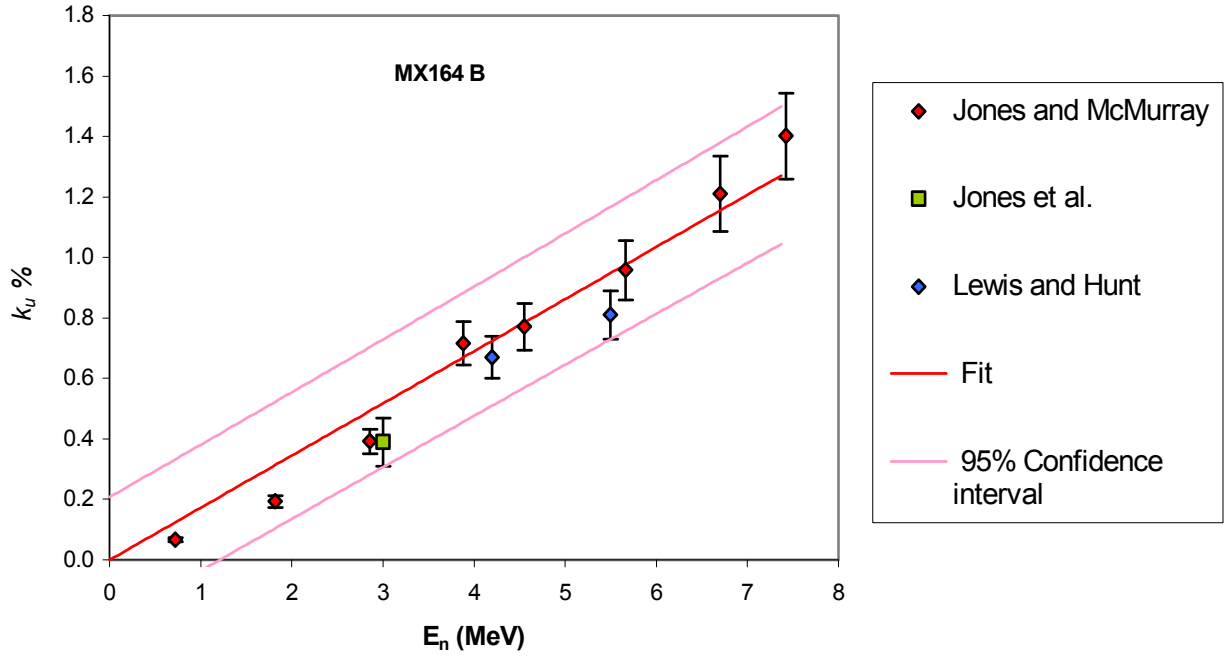

Figure 5. Plot of neutron sensitivity of MX164 detector; data taken from Jones and McMurray [20], Jones *et al.* [21], and Lewis and Hunt [22].

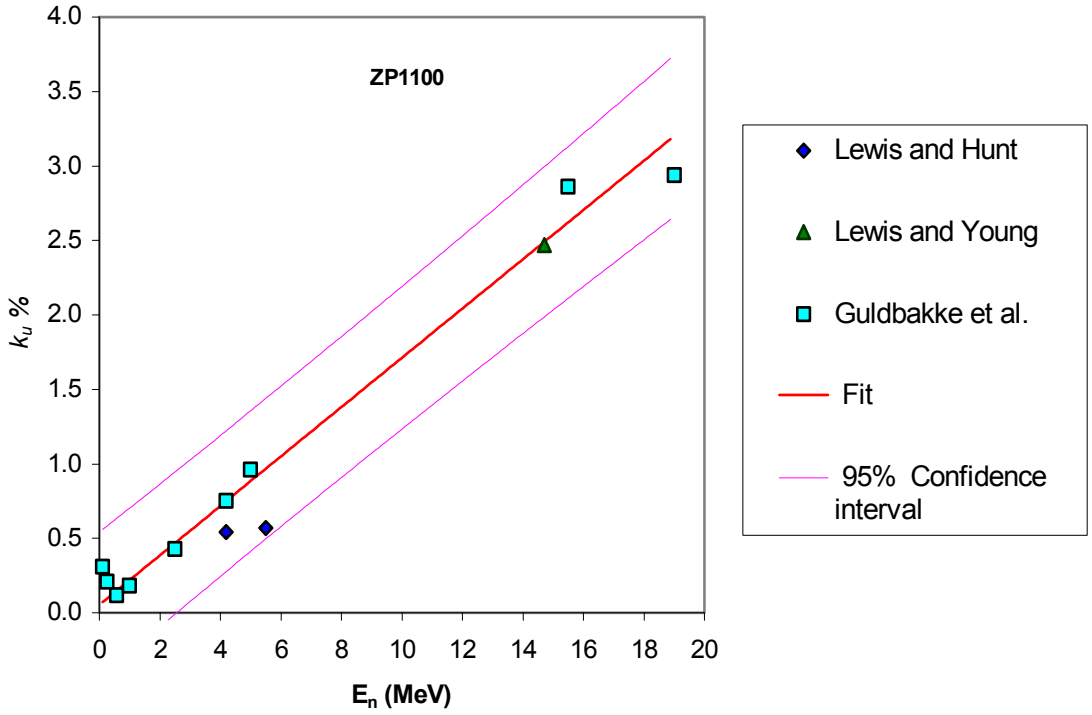

Figure 6. Plot of neutron sensitivity of ZP1100 detector; data taken from Lewis and Hunt [22], Lewis and Young[23], and Guldbakke *et al.* [24].

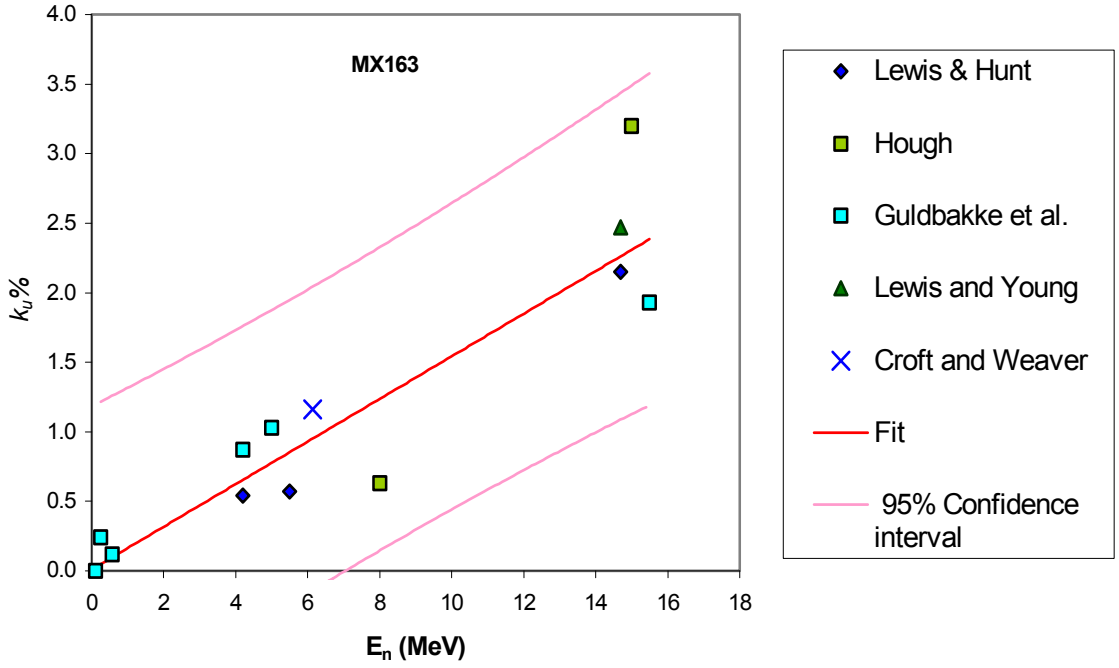

Figure 7. Plot of fast neutron sensitivity of the MX163 detector, data taken from Lewis and Hunt [22], Hough [25], Guldbakke *et al.* [24], Lewis and Young [23], and Croft and Weaver [26].

The MX164B and MX164A have similar constructions, although the Perspex® used in the MX164A has been replaced by PTFE in the MX164B. The reduced hydrogen content of the PTFE might be expected to reduce the neutron response of the MX164B relative to the MX164A by reducing the probability of hydrogen capture in the detector leading to a decrease in the gamma radiation striking the counter. However, for fast neutrons, this effect is expected to be small, as few of these neutrons are captured, and the literature indicates that any difference is negligible. (The effective photon detection probability for Geiger detectors, defined as the ratio of the counts recorded to the number of photons striking it, is about 0.5%.)

The figures show the relative neutron sensitivity, k_u, of the MX164, ZP1100 and MX163 detectors for various neutron energies. For all three types of Geiger-Müller tube the k_u value appears to increase linearly with energy. A linear fit has been made to the data and the corresponding 95% confidence intervals are shown. This reveals that the ZP1100 has the highest k_u value, and the MX163 the lowest over the relevant energy range. The available data for the MX163 has a poor correlation and the linear fit is poor, but upper limits can still be defined.

The k_u of the most sensitive tube, the ZP110, to the 4.2 MeV mean neutron energy of the highest energy source, ^{241}Am-Be, is predicted to be 0.0075 ± 0.0050. As a result it has been assumed in the first instance that the neutron response of all the detectors over the energy range of interest is insignificant. Confirmation of this can only come from the final results for relative photon and neutron dose or kerma values in the fields of interest.

2.5 Electronic set up of the Geiger-Müller detectors

The electronic arrangement used to operate all four Geiger-Müller counters is shown in Figure 8 and was used for all measurements. Each detector was connected to a Harwell 3792 Gamma Monitor System via an RG 58 cable no longer than 2 m. The pulse output of the 3792 was passed into a width/delay unit via a ~50 m coaxial cable. The width delay unit was used to generate a pulse acceptable to a PC scaler unit and to impose a known dead-time on the system following each detector count. The PC scaler recorded the number of pulses from the width/delay unit and allowed both the total counting time and the individual sampling time to be set. The oscilloscope was used to compare the detector and width/delay pulses during the initial set up, but was disconnected during measurements.

For all detectors a voltage of 575 V was applied to the anode, and regular checks of the voltage stability were made between measurements. An internal jumper within the Harwell 3792 electronics was set to provide a time constant for the coupling circuit of 1 μs. This produced a 1 V negative pulse and was found to be the optimum configuration for use with the width/delay unit. Pulses for all four detectors were observed to have a ~5 μs rise time. The fall time of the pulse for the MX164A and MX164B was observed to be ~55 μs and for the ZP1100 and MX163 it was observed to be ~25 μs. To prevent pile-up the width/delay unit was set so that its output pulse fully encompassed the pulse from the Harwell 3792. As a result, a dead-time of 60 μs was set for the MX164s and 30 μs for the ZP1100 and MX163. For the low count rates encountered in these measurements dead-time corrections were made using the non-paralyseable assumption [27].

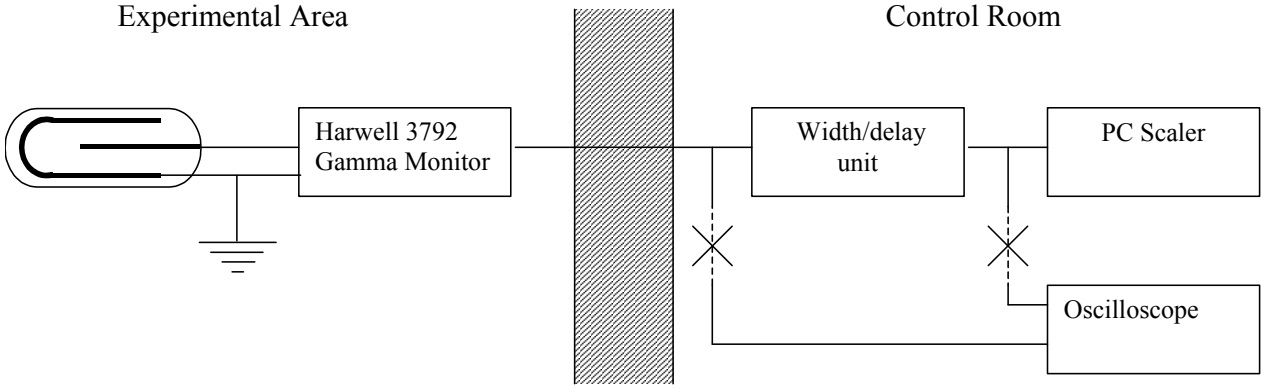

Figure 8. Electronic set-up for measurements using Geiger-Müller detectors.

2.6 Geiger-Müller photon response measurement

Sensitivity calibrations of the Geiger-Müller detectors were performed at NPL's multi-source photon irradiation unit. The individual detectors were mounted with their axes perpendicular to known photon fields generated by collimated ^{241}Am, ^{137}Cs and ^{60}Co sources. To improve repeatability, the radial orientation of each detector with respect to the source was marked. Where practicable the source activity and source-detector distance were chosen to provide a similar air kerma rate as those expected during the mixed n-γ field measurements.

The air kerma rate in each field was measured using an NPL primary standard ion chamber the details of which are described by CIRM Report 53 [28]. Where necessary air kerma rates measured by the ion chamber were corrected for changes in geometry and air attenuation

arising from any difference in location between the two detectors. This allowed the air kerma response of the detectors to be measured at the centre of the detectors. The resulting relative uncertainty in the measurement of air kerma rates was estimated to be <0.5%.

The detector responses between 33 and 250 keV were measured using the ISO narrow series of X-ray qualities [29] listed in Table 2. The measurements were performed using NPL's 300 kV X-ray facility with the set up described in Section 2.5. The detectors were mounted perpendicular to the field with the same radial orientation as used during the calibration with photon sources.

Table 2. X-ray qualities used for GM tube calibration

X-ray quality	Mean energy (keV)	Spectral width (keV)
40 kV	33	10
60 kV	48	18
80 kV	65	22
100 kV	83	23
120 kV	100	28
150 kV	118	46
200 kV	164	52
250 kV	208	58
300 kV	250	74

The air kerma rate for each X-ray quality was measured using an NPL ion chamber as a transfer standard from the NPL primary standard free air ion chamber, which could not directly measure the low dose rates used. Air kerma rates measured by the ion chamber were corrected for changes in geometry and air attenuation arising from any difference in location between the two detectors. The resulting relative uncertainty in the measured air kerma rate was 3%.

2.7 Measurement of photon doses in mixed fields using Geiger detectors

Measurements of the neutron sources detailed in Table 1 were performed in NPL's low scatter facility in the Chadwick Building. This room is 23 m long, 17 m wide and 18 m high. It has ~1 m thick concrete shield walls and a ~25 cm thick concrete roof. Sources were mounted 6 m above the floor and 7 m from the nearest wall. Access to the source and detectors was via low-density walkways.

Using a retort stand, two detectors at a time were mounted at two locations P1 and P2, both at approximately 75 cm from the source, as shown in Figure 9. P1 and P2 had a horizontal separation from each other of 30 cm. The resulting uncertainty in the source to detector distance was 2 mm. The detectors were positioned with their cylindrical axes perpendicular to the radiation field and with their axes in the same radial orientation as during calibration.

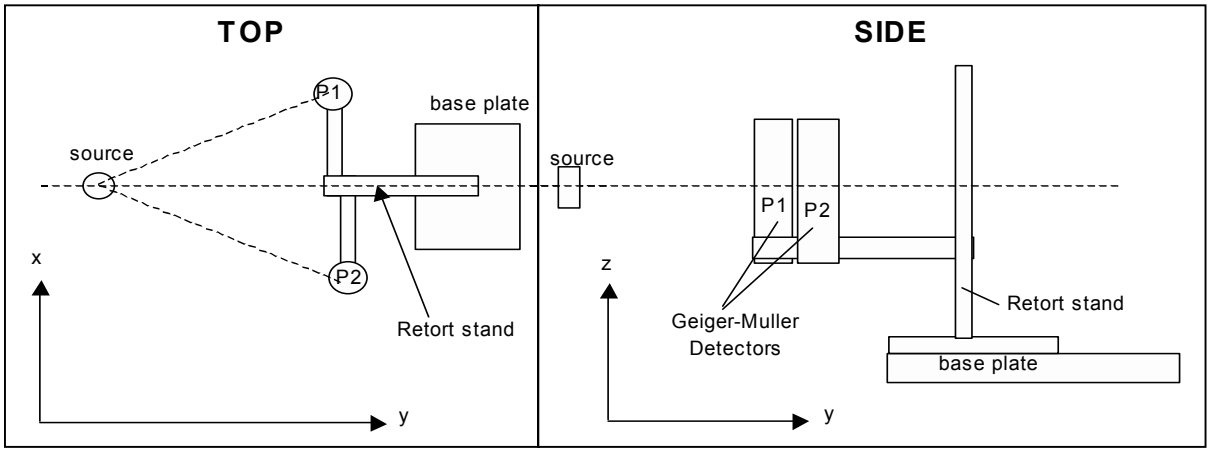

Figure 9. Experimental arrangement for neutron source measurements using Geiger-Müller detectors.

Measurements were made using the electronic set-up described in Section 2.5. The PC scaler recorded the counts every 30 s and samples were automatically repeated. Where practicable measurement times were chosen to achieve, where possible, a statistical uncertainty of less than 1% on the total counts. For low count rates this could not be achieved in a reasonable time and the statistical uncertainty was limited by the time available for measurement.

In-situ background measurements were made before and after the source measurements the mean of which was used for background correction.

2.8 Photon dose measurements in mixed fields with electronic personal dosemeters

For comparison, measurements of the photon component in NPL's standard radionuclide neutron fields were also performed using four Thermo Electron EPD MkII and four EPD-N2 dosemeters.

The EPDs and EPDN2s where mounted on the front face of an ISO water phantom. The front face of the phantom was perpendicular to the radiation field and at a distance of 75 cm from the centre of the source. The EPDs were arranged as shown in Figure 10. Measurements were made of all the sources listed in Table 1 with the exception of ^{241}Am-Li with lead.

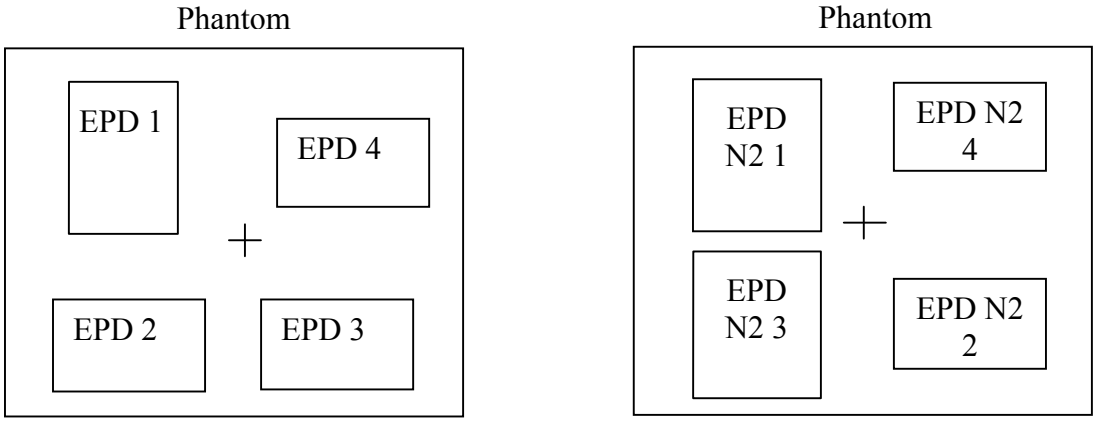

Figure 10. Identity and location of electronic personal dosemeters on phantom

Due to a lack of knowledge of the effective centre of the dosemeters, a ± 2 cm uncertainty in the distance from the dosemeter to the centre of the phantom face (radial distance) was assumed. The radial distances used are given in Table 3.

Table 3. Electronic personal dosemeters used in on-phantom measurements

Dosemeter	EPD ID	Radial Distance from centre of phantom (cm)	Dosemeter	EPD ID	Radial Distance from centre of phantom (cm)
EPD 1	00073611	7.5	EPD N2 1	07101900	8.7
EPD 2	00073613	7.6	EPD N2 2	07101216	8.5
EPD 3	00073612	7.4	EPD N2 3	07101763	8.5
EPD 4	00073614	6.8	EPD N2 4	07101797	8.7

The dose indicated by each dosemeter was recorded every 10 s and the statistical uncertainty calculated from the fluctuation in recorded dose rate throughout the measurement. Measurement time varied but was typically longer than 10 hours and for the 37 GBq ^{241}Am-F source, measurements were taken continuously for 2 days.

3 RESULTS AND DISCUSSION

3.1 Photon response calibrations of Geiger-Müller counters

The Geiger detector responses measured with ^{241}Am, ^{137}Cs, ^{60}Co and medium energy X-ray qualities are shown in Figure 11 and tabulated in Appendix C. Measurements were corrected for dead-time and background and have been normalised so that the ^{60}Co result is unity. The X-ray data values have been plotted at the mean energy of the distribution.

Figure 11 also shows continuous response curves. These were derived from the discrete data by four-point cubic Lagrangian interpolation against the logarithm of the photon energy. To estimate the detector response to photons above 1.25 MeV generic response data for the MX164A, MX164B and MX163 detectors were included for 6 MeV photons measured at Hinkley Point A power station [30]. This originates from ^{16}N gamma emissions mainly at 6.13 MeV. The response was set as 0 for photons of less than 20 keV to maintain a realistic estimate for the detector response below 33 keV. This results in a smooth and realistic response function for each detector.

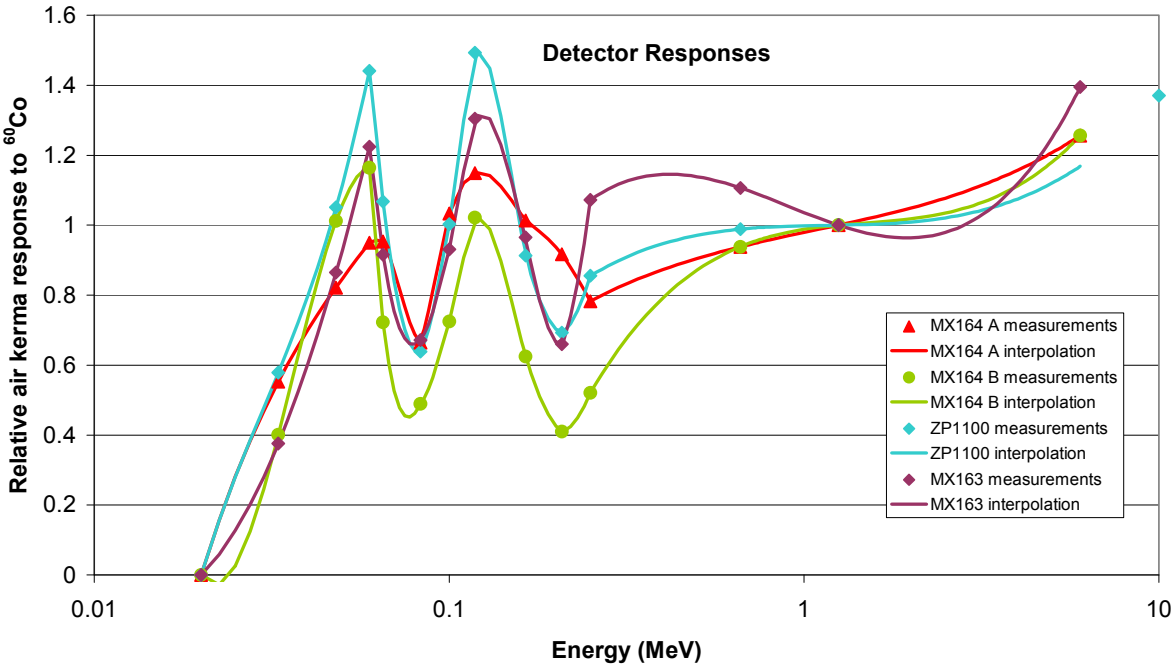

Figure 11. Air kerma response of Geiger-Müller detectors relative to ^{60}Co.

The resulting functions are a good estimate of the responses for these detectors over an energy range 0 to 6 MeV. The response rapidly increases from the starting energy up to a maximum for 60 keV photons. The similarity of the ^{137}Cs sensitivity to that for ^{60}Co means that the response is approximately flat from 200 keV to 1.25 MeV; it then increases with increasing photon energy. For photon energies above 1.25 MeV the data are limited and the response in this region is only tentative.

Previous measurements using these Geiger-Müller detectors [22] frequently assumed the response was flat to within 10% between 60 keV and 1.2 MeV. From Figure 11 it is clear that this is not the case for these detectors and to achieve accurate results it is vital to perform a correction for each detector's relative response.

The photon fluence spectra, detailed in Appendix A for ^{241}Am-based sources and in Appendix B for ^{252}Cf, were converted to fractional air kerma spectra using the conversion coefficients for air kerma per unit fluence tabulated in ICRP 74 [31], or identically in ICRU 57 [32]. The detector response curve *R(E)* was then used to calculate the effective sensitivity h_u for a particular source, relative to ^{60}Co, by:

$$h_u = \sum R(E_i) K_i \qquad (2)$$

where K_i is the normalised air kerma contribution of each photon component, *i,* from a source and $R(E_i)$ is the sensitivity of the detector, relative to ^{60}Co, at the photon energy E_i of component *i*. The resulting h_u values for each detector and source are listed in Table 4.

A full treatment of the uncertainty associated with the effective relative response of each detector is not trivial. Instead conservative estimates of the uncertainty have been used based on the quality of the information available about the dominant components. As a result an arbitrary uncertainty of 3% on the effective relative sensitivity values (h_u) has been assumed. The ^{241}Am-Be source with lead filter is an exception, because its spectrum is dominated by 4.439 MeV gamma rays, which are in a poorly known region of the response curve. As a result an uncertainty of 10% has been assumed on each detector's effective relative response to lead filtered ^{241}Am-Be.

Table 4. The effective relative sensitivity of each detector to the photons from the range of neutron sources studied. These values are calculated from the product of the normalised air kerma photon spectra of each source and the interpolated detector sensitivity curves and are relative to ^{60}Co.

Source	Detector				Assumed uncertainty
	MX164A	MX164B	ZP1100	MX163	
^{241}Am-Be	0.95	1.16	1.43	1.22	3%
^{241}Am-Be(Pb)	1.07	1.04	1.05	1.14	10%
^{241}Am-Li	0.94	1.15	1.43	1.21	3%
^{241}Am-Li(Pb)	0.89	0.79	0.95	1.11	3%
^{241}Am-B	0.94	1.16	1.43	1.22	3%
^{241}Am-F	0.94	1.16	1.43	1.22	3%
^{252}Cf	0.97	0.94	0.99	1.06	3%
D_2O mod ^{252}Cf	1.01	1.00	1.01	1.03	3%

3.2 Photon dose measurements in mixed fields using Geiger tubes

The dead-time and background corrected air kerma rates free in air at 75 cm were measured with all four detectors for the various neutron sources and are presented in Table 5. The values contained in Table 4 were used to derive the effective detector response to each source and hence calculate the air kerma rates. For consistency the dead-time corrected count rates measured by the Geiger-Müller counters in the various mixed fields were corrected to a distance of 75 cm from the source. These distance corrections were less than 2 cm and so changes in air attenuation and build up are negligible. Dead-time corrections for all measurements were less than 1%.

Table 5. Photon air kerma rates at 75 cm from neutron sources measured by Geiger-Müller detectors. Uncertainties in the least significant digit are given in parentheses.

Detector ID	Measured air kerma rate (μGy h^{-1})							
	^{241}Am-Be	^{241}Am-Be (Pb)	^{241}Am-Li	^{241}Am-Li (Pb)	^{241}Am-B	^{241}Am-F	^{252}Cf	D_2O mod ^{252}Cf
MX164A	91 (3)	20 (2)	46 (2)	0.67 (3)	9.7 (3)	8.4 (3)	6.3 (2)	4.4 (2)
MX164B	81 (3)	21 (2)	42 (1)	0.75 (3)	9.2 (3)	7.4 (2)	6.4 (2)	4.6 (2)
ZP1100	80 (3)	18 (2)	47 (2)	0.69 (3)	9.9 (3)		6.1 (2)	4.5 (2)
MX163	79 (3)	17 (2)	46 (2)	0.71 (3)			6.7 (3)	4.8 (3)

Figure 12 shows the variation of each detector's measurement from the weighted mean for each source. The spread of results is consistent with the calculated uncertainty and primarily stems from uncertainty in the effective relative sensitivities. This is a result of uncertainty in the assumed photon spectrum of each source and is predominantly a systematic error for each detector.

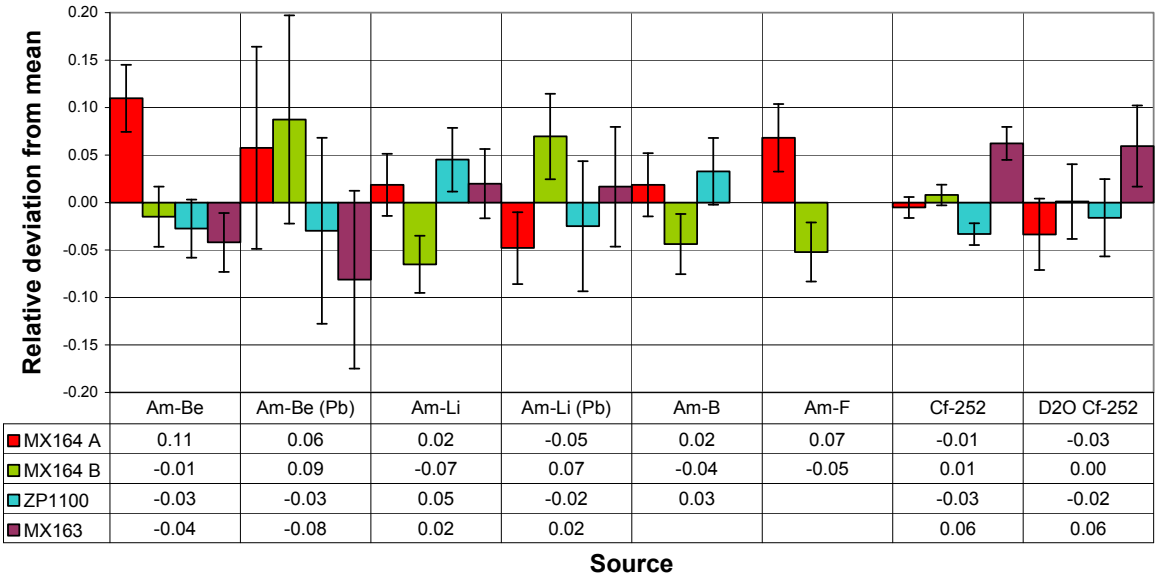

	Am-Be	Am-Be (Pb)	Am-Li	Am-Li (Pb)	Am-B	Am-F	Cf-252	D2O Cf-252
MX164 A	0.11	0.06	0.02	-0.05	0.02	0.07	-0.01	-0.03
MX164 B	-0.01	0.09	-0.07	0.07	-0.04	-0.05	0.01	0.00
ZP1100	-0.03	-0.03	0.05	-0.02	0.03		-0.03	-0.02
MX163	-0.04	-0.08	0.02	0.02			0.06	0.06

Figure 12. Variation of Geiger-Müller measurements of photon air kerma.

The weighted mean values of the air kerma rates measured by the Geiger tubes are presented in Table 6. By folding the photon air kerma spectra with the kerma to dose equivalent

conversion coefficients detailed in ICRP 74 [31]/ICRU 57 [32] the photon personal dose equivalent rate $\dot{H}_p(10)_\gamma$ and photon ambient dose equivalent rate $\dot{H}^*(10)_\gamma$ were calculated. These are also shown in Table 6. The uncertainty in these calculated values stems primarily from the uncertainty in the photon spectrum. This is already considered as part of the effective relative detector sensitivity and so is not considered in the dose conversion coefficients which are conventionally assumed to be exact. Absorbed photon dose rate in ICRU muscle was calculated using tabulated mass energy absorption coefficients from ICRU 44 [33].

The values of $\dot{H}_p(10)_\gamma$ and $\dot{H}^*(10)_\gamma$ for the unshielded ^{241}Am sources are consistently greater than the corresponding kerma or absorbed dose rate values for the same sources. This stems from the large 60 keV photon contributions, for which the ICRP 74 kerma to $\dot{H}_p(10)_\gamma$ or $\dot{H}^*(10)_\gamma$ conversion coefficients are significantly larger than at higher energies.

Table 6. Mean photon air kerma, absorbed dose, and dose equivalent rates at 75 cm measured by Geiger-Müller tubes, and photon/neutron dose equivalent ratios for neutron sources.

Source	Mean air kerma rate (μGy h^{-1})	Tissue absorbed dose rate $\dot{D}_\gamma$ (μGy h^{-1})	$\dot{H}_p(10)_\gamma$ (μSv/h)	$\dot{H}^*(10)_\gamma$ (μSv/h)	$\frac{\dot{D}_\gamma}{\dot{D}_n}$	$\frac{\dot{H}_p(10)_\gamma}{\dot{H}_p(10)_n}$	$\frac{\dot{H}^*(10)_\gamma}{\dot{H}^*(10)_n}$
^{241}Am-Be	82(3)	88(3)	154(5)	142(5)	1.3(3)	0.221(9)	0.214(9)
^{241}Am-Be (Pb)	18.9(9)	21(1)	22(1)	22(1)	0.31(2)	0.031(2)	0.033(2)
^{241}Am-Li	45(1)	48(1)	85(2)	78(2)	312(60)	30(1)	28(1)
^{241}Am-Li (Pb)	0.70(2)	0.77(2)	0.92(2)	0.89(2)	5.0(9)	0.32(2)	0.32(2)
^{241}Am-B	9.6(2)	10.3(2)	18.0(4)	16.6(3)	13(3)	1.87(8)	1.79(8)
^{241}Am-F	7.8(3)	8.4(3)	14.7(7)	13.6(7)	45(9)	5.0(3)	4.8(3)
^{252}Cf	6.35(9)	7.0(1)	7.6(1)	7.5(1)	0.7(2)	0.057(2)	0.059(2)
D_2O ^{252}Cf	4.56(9)	5.0(1)	5.3(1)	5.3(1)	2.6(6)	0.167(8)	0.176(8)

Also shown in Table 6 is the ratio of photon to neutron dose equivalent rate values. For ^{241}Am-Be, ^{241}Am-B, ^{252}Cf and D_2O moderated ^{252}Cf the neutron ambient dose equivalent rate, $\dot{H}^*(10)_n$, and personal dose equivalent rate, $\dot{H}_p(10)_n$, were calculated from the free-field neutron fluence rate using the spectrum averaged fluence-to-dose conversion coefficients given by ISO 8529-1 [1]. For the ^{241}Am-Li source these quantities were calculated using the conversion coefficients calculated by Tagziria *et al.* [12] For the ^{241}Am-F source the coefficients were taken to be those for the mean of the two measurements by Owen and by Tagziria [10,11]. The neutron absorbed dose rate was calculated from the tabulated fluence-to-kerma conversion coefficients for ICRU muscle, which was assumed to be equivalent to absorbed dose. ICRU 63 [34] recommends an uncertainty of 20% for these kerma coefficients, and this component dominates the uncertainty in the absorbed dose ratio.

In all cases, the free field neutron fluence was decay-corrected from the date of the most recent source emission rate measurement, the uncertainty in which was typically 1%. Uncertainties in the fluence spectra and differences in source encapsulation mean that the dose equivalent conversion coefficients for individual sources may deviate slightly from the above values. According to ISO 8529-2 [35], these uncertainties may be taken as being ± 1% for bare ^{252}Cf and ± 4% for the other sources.

With the availability of the photon to neutron dose ratio information the question of whether the neutron sensitivity of the Geiger-Müller tubes can be neglected can be resolved. The maximum neutron response will be for the ^{241}Am-Be behind lead. Taking the dose ratio of 0.31 from Table 6 and the k_u value of 0.0075 from section 2.4 the maximum effect is about 2.5%. This is within the quoted uncertainties and all other neutron responses will be significantly smaller.

The ratios of photon and neutron personal dose equivalent components, where the photon component was measured by the EPDs and EPD-N2s positioned on an ISO water phantom at 75 cm from the source, are shown in Table 7. Neutron dose equivalents were calculated from the free-field fluences (not the EPD-N2 results). Where no data is shown no measurements were performed for that source.

Table 7. $\dot{H}_p(10)_\gamma / \dot{H}_p(10)_n$ dose equivalent rate ratios based on photon rates measured with EPDs.

Detector ID	Ratio of $\dot{H}_p(10)_\gamma$ (measured) to $\dot{H}_p(10)_n$ (derived from the free field fluence rate)						
	^{241}Am-Be	^{241}Am-Be (Pb)	^{241}Am-Li	^{241}Am-B	^{241}Am-F	^{252}Cf	D_2O mod ^{252}Cf
EPD 1	0.206 (2)		29.5 (0.4)	1.78 (8)	4.9 (3)	0.050 (3)	0.125 (9)
EPD 2	0.203 (2)		28.6 (0.4)	1.68 (8)	4.7 (2)	0.050 (3)	0.126 (9)
EPD 3	0.208 (2)		29.7 (0.4)	1.77 (8)	4.9 (2)	0.049 (3)	0.127 (9)
EPD 4	0.199 (2)		28.1 (0.4)	1.70 (8)	4.7 (2)	0.050 (3)	0.128 (9)
EPDN2 1	0.208 (2)	0.0321 (2)			5.0 (2)	0.056 (2)	
EPDN2 2	0.206 (2)	0.0324 (2)			4.9 (2)	0.056 (2)	
EPDN2 3	0.208 (2)	0.0327 (2)			5.0 (2)	0.056 (2)	
EPDN2 4	0.209 (2)	0.0327 (2)			5.0 (2)	0.056 (2)	

The uncertainties in Table 7 are derived simply from the statistics on repeated measurements and thus do not represent a true estimate of the uncertainty in the gamma to neutron ratio. It can, however, be seen that the results of the different EPDs are consistent, the agreement being roughly within the statistical uncertainties indicating very similar calibrations for individual dosemeters.

Table 8 shows the mean EPD values compared with the equivalent ratios measured by the Geiger-Müller tubes. The uncertainties shown in this table for the EPDs were derived from the mean of the observed statistical fluctuations during the measurements, but also include geometry uncertainty and the uncertainty in the neutron fluence-to-dose equivalent conversion coefficients. They do not include the uncertainty in the photon calibration (unknown), potential systematic uncertainty arising from the variation in photon response with energy, or from potential cross-contamination of the photon and neutron channels.

Table 8. Weighted mean of the Geiger-Müller counter and electronic personal dosemeter measurements of $\dot{H}_p(10)_\gamma / \dot{H}_p(10)_n$

Detector type	Ratio of $\dot{H}_p(10)_\gamma$ (measured) to $\dot{H}_p(10)_n$ (derived from free field fluence rate)						
	^{241}Am-Be	^{241}Am-Be (Pb)	^{241}Am-Li	^{241}Am-B	^{241}Am-F	^{252}Cf	D_2O mod ^{252}Cf
Mean of GM measurements	0.221 (9)	0.031 (2)	30 (1)	1.87 (8)	5.0 (3)	0.057 (2)	0.167 (8)
Mean of EPD measurements	0.20 (1)		29 (2)	1.7 (1)	4.8 (3)	0.050 (3)	0.13 (1)
Mean of EPD-N2 measurements	0.21 (1)	0.032 (2)			5.0 (3)	0.056 (2)	

Generally the electronic personal dosemeter measurements agree very well with the Geiger-Müller counter measurements. This indicates that both the EPD and EPD-N2 are suitable instruments for the measurement of the photon dose in standard radionuclide produced neutron fields and offer an easy method of measuring the photon doses in neutron fields.

Further improvements to the measurements using electronic personal dosemeters could be made by folding the source photon spectra into the dosemeter photon response. However, time restrictions prevented greater depth in the analysis.

3.3 Summary

The ^{241}Am-Li source has the largest ratio of photon to neutron dose, with the neutron component making up only 3% of the total $H_p(10)$ dose. The ^{241}Am-Li photon spectrum has numerous high-energy photon components. Thus, even though the use of a 2 mm lead filter was shown to reduce the dose by a factor of 100, the low neutron yield and significant high energy photon component mean that the photon dose component is still 23% of the total dose even with the lead filter.

The higher neutron yield per ^{241}Am decay from the ^{241}Am-Be source means that when behind the lead filter it produces the smallest photon component relative to the neutron component of the measured sources, although the absolute photon dose rate from the shielded 555 GBq source is still higher than that from unshielded 37 GBq ^{241}Am-B and ^{241}Am-F sources.

Table 9 compares the present measurements with earlier measurements by McDonald *et al.*[2], Spurný *et al.* [3], Józefowicz [4], and Langner *et al* [5]. The results for the present work are those from the Geiger-Müller counter measurements as they are expected to be the most reliable.

The result of McDonald *et al*. is based on gamma dose measurements with a Geiger-Müller counter, a tissue equivalent proportional counter (TEPC), and thermoluminescence dosemeters (TLDs). The neutron dose was determined from both a TEPC measurement, and by subtracting the gamma dose from the total dose as measured using a tissue equivalent ionisation chamber. Neutron dose was converted to dose equivalent using a quality factor for the D_2O moderated ^{252}Cf spectrum, and it was assumed that gamma dose equivalent was identical to the gamma dose. It should be noted that this work was performed prior to the introduction of the operational quantities $H_p(10)$ and $H^*(10)$, although conversion

coefficients from neutron fluence to dose equivalent have not changed dramatically over the years as the various new dose equivalent quantities have been introduced [36]. In view of the different assumptions, however, and the fact that the photons from a D_2O moderated ^{252}Cf source will depend on the age of the source, the agreement with the present measurement is probably simply fortuitous.

Table 9. Comparison with previous measurements

Source	This work. G-M counter data $H^*(10)_\gamma / H^*(10)_n$	Previous measurements			
		McDonald *et al.* [2] (1984)[a]	Spurný *et al.* [3]† (1997)[b]	Józefowicz [4] (2004)[c]	Langner *et al.* [5]† (2007)[d]
^{241}Am-Be (Pb)	0.033 ± 0.002		0.033 ± 0.005	0.034	0.027 ± 0.003
^{241}Am-Li(Pb)	0.32 ± 0.02		0.34 ± 0.05		
^{252}Cf	0.059 ± 0.002		0.038 ± 0.005	0.048	0.043 ± 0.003
D_2O ^{252}Cf	0.176 ± 0.008	0.18 ± 0.03	0.12 ± 0.02		0.142 ± 0.012

a Quantity described as "ratio of gamma dose to neutron dose equivalent"
b Quantity is ratio of $H^*(10)$ values
c Ratio of gamma dose to neutron $H_p(10)$. Mean of three measurements with two different instruments.
d Ratio of $H^*(10)$ values
† The uncertainties quoted by these authors in their paper are at the 2σ sigma confidence limit, i.e. at a confidence interval $k = 2$. For presentation here they have been reduced by a factor of 2 for consistency with the other uncertainties all of which are given at $k = 1$.

Comparison of the present results with those of Spurný *et al.*[3]. reveals good agreement for ^{241}Am-based sources with poor agreement for ^{252}Cf and D_2O moderated ^{252}Cf. This may reflect differences in the age of the ^{252}Cf sources. The photon emission from a ^{252}Cf source depends on its age. Fission products build up with time increasing the photon to neutron dose equivalent ratio. The NPL ^{252}Cf source measured in this work is particularly old having been at the lab for 22 years. The probability of the sources having different ages provides a qualitative explanation of the difference, but to provide a full quantitative explanation of the differences information about the age of the sources and about the exact nature of the fission product build-up would be needed.

The data of Spurný *et al.* is based on photon measurements with a TEPC, scintillators, a set of Geiger-Müller counters, a silicon diode, and TLDs. For the neutrons the dose equivalent was determined with a TEPC, two area survey instruments, and bubble detectors. The range of different devices used give the data good credibility although derivation of the neutron dose equivalent from accurately known source emission rates, as was done in the present work, provides higher accuracy.

The results of Józefowicz[4] are based on photon dose measurements with both a high pressure Al-CO_2 ionisation chamber and a tissue-equivalent recombination chamber. No neutron dose equivalent values are quoted and the ratios presented in Table 9 were derived by estimating the neutron dose equivalent from the quoted emission rates for the sources used.

Again the agreement for the ^{241}Am-based source is good although that for ^{252}Cf is rather poor. Again the age of the sources may be a contributory factor to the difference.

The recent data of Langner *et al.*[5]. is particularly interesting as they performed their photon measurements with a Geiger-Müller counter and did not assume a flat photon air kerma response. In a manner similar to the approach in the present report they have used a measured air kerma response and corrected the Geiger-Müller counter response for the spectrum of the gamma rays from the sources measured. The results for the lead shielded ^{241}Am-Be source are in reasonable agreement with the present measurements. For the ^{252}Cf and D_2O moderated ^{252}Cf sources the results of Langer *et al*. are lower than the present measurements, but again the relative ages of the sources may explain these differences.

International standard ISO 8529-1[1] quotes values of 0.18 for the "ratio of photon to neutron dose equivalent rates" for D_2O moderated ^{252}Cf (presumably from the measurements of McDonald *et al*.) 0.05 for ^{252}Cf, < 0.2 for ^{241}Am-B with lead, and < 0.05 for ^{241}Am-Be with lead. The origin of the last three values is not clear. These data are reasonably consistent with the present results, but any future revision of this standard could include improved data on the photon components in these standard radionuclide source produced neutron fields.

4 CONCLUSIONS

The free-in-air photon doses at 75 cm from a range of radioisotope based neutron sources have been measured with uncertainties of typically 3%. These measurements involved a more detailed treatment of the photon fields and photon detector responses than most previous measurements of this type. This will allow NPL to extend its capabilities to include measurements of the neutron response of photon sensitive detectors provided either the photon response function is available or the device has a truly photon dose equivalent or air kerma response.

Measurements of NPL accelerator-based sources will allow a similar capability to be expanded to include the NPL monoenergetic neutron fields.

5 ACKNOWLEDGEMENTS

The technical assistance and equipment provided by Mike Bates of Centronic Ltd. is greatly appreciated. This work was funded by the UK National Measurement System Policy Unit in its Programme for Ionising Radiation Monitoring Metrology from 2004 to 2007.

Appendix A: ^{241}Am(α,n) source photon spectra

Attenuation-corrected photon fluence spectra for the ^{241}Am-based neutron sources. These were used to derive the effective detector sensitivities and dose conversion coefficients. The composition of each spectrum and the attenuation correction is described in Sections 2.2 and 2.3. Plots of the ^{241}Am-Be spectrum without lead shielding and of the ^{241}Am-Li spectrum with lead shielding are presented in Figure 13 and Figure 14 respectively.

Table 10. Relative intensities for gamma ray lines for radionuclide neutron sources based on ^{241}Am

^{241}Am-Be		^{241}Am-Be (Pb)		^{241}Am-B	
E **(MeV)**	**Normalised fractional fluence**	***E*** **(MeV)**	**Normalised fractional fluence**	***E*** **(MeV)**	**Normalised fractional fluence**
0.0332	9.7×10^{-8}	0.0595	2.3×10^{-2}	0.0332	9.7×10^{-8}
0.0427	3.0×10^{-6}	0.0697	1.8×10^{-4}	0.0427	3.0×10^{-6}
0.0433	5.0×10^{-5}	0.0758	2.2×10^{-4}	0.0433	5.0×10^{-5}
0.0595	9.9×10^{-1}	0.0989	1.2×10^{-5}	0.0595	9.9×10^{-1}
0.0697	2.0×10^{-4}	0.102	3.2×10^{-5}	0.0697	2.0×10^{-4}
0.0758	5.8×10^{-5}	0.114	1.5×10^{-5}	0.0758	5.8×10^{-5}
0.0970	2.1×10^{-4}	0.123	1.8×10^{-4}	0.0970	2.1×10^{-4}
0.0989	3.9×10^{-3}	0.125	1.0×10^{-3}	0.0989	3.9×10^{-3}
0.101	3.6×10^{-4}	0.146	1.3×10^{-3}	0.101	3.6×10^{-4}
0.102	4.0×10^{-3}	0.166	1.7×10^{-3}	0.102	4.0×10^{-3}
0.113	4.7×10^{-5}	0.169	7.0×10^{-3}	0.113	4.7×10^{-5}
0.114	1.0×10^{-4}	0.208	4.5×10^{-2}	0.114	1.0×10^{-4}
0.123	2.6×10^{-4}	0.250	1.4×10^{-2}	0.123	2.6×10^{-4}
0.125	1.1×10^{-3}	0.326	6.9×10^{-2}	0.125	1.1×10^{-3}
0.146	1.4×10^{-4}	0.335	1.2×10^{-1}	0.146	1.4×10^{-4}
0.169	5.9×10^{-5}	0.368	5.5×10^{-2}	0.169	5.9×10^{-5}
0.208	2.7×10^{-4}	0.375	2.6×10^{-2}	0.208	2.7×10^{-4}
0.326	1.2×10^{-4}	0.376	3.9×10^{-2}	0.326	1.2×10^{-4}
0.335	1.9×10^{-4}	0.619	2.5×10^{-2}	0.335	1.9×10^{-4}
0.368	8.0×10^{-5}	0.648	6.4×10^{-2}	0.368	8.0×10^{-5}
0.376	5.5×10^{-5}	0.662	1.6×10^{-1}	0.376	5.5×10^{-5}
0.619	2.6×10^{-5}	0.722	8.9×10^{-2}	0.619	2.6×10^{-5}
0.662	1.6×10^{-4}	0.756	1.4×10^{-2}	0.662	1.6×10^{-4}
0.722	8.8×10^{-5}	4.439	2.2×10^{-1}	0.722	8.8×10^{-5}
4.439	2.0×10^{-4}			2.313	4.1×10^{-5}
				3.684	5.8×10^{-5}
				3.854	2.4×10^{-5}
				4.439	9.2×10^{-7}

Table 10. Continued

^{241}Am-Li		^{241}Am-Li (Pb)		^{241}Am-F	
E **(MeV)**	**Normalised fractional fluence**	***E*** **(MeV)**	**Normalised fractional fluence**	***E*** **(MeV)**	**Normalised fractional fluence**
0.0427	3.0×10^{-6}	0.0595	1.4×10^{-2}	0.0332	9.7×10^{-8}
0.0433	5.0×10^{-5}	0.0697	1.1×10^{-4}	0.0427	3.0×10^{-6}
0.0595	9.9×10^{-1}	0.0758	1.3×10^{-4}	0.0433	5.0×10^{-5}
0.0697	2.0×10^{-4}	0.0989	7.1×10^{-6}	0.0595	9.9×10^{-1}
0.0758	5.7×10^{-5}	0.102	1.9×10^{-5}	0.0697	2.0×10^{-4}
0.0970	2.1×10^{-4}	0.114	8.9×10^{-6}	0.0758	5.8×10^{-5}
0.0989	3.9×10^{-3}	0.123	1.1×10^{-4}	0.0970	2.1×10^{-4}
0.101	3.6×10^{-4}	0.125	6.0×10^{-4}	0.0989	3.9×10^{-3}
0.102	4.0×10^{-3}	0.146	7.8×10^{-4}	0.101	3.6×10^{-4}
0.113	4.7×10^{-5}	0.166	1.0×10^{-3}	0.102	4.0×10^{-3}
0.114	1.0×10^{-4}	0.169	4.2×10^{-3}	0.113	4.7×10^{-5}
0.123	2.6×10^{-4}	0.208	2.7×10^{-2}	0.114	1.0×10^{-4}
0.125	1.1×10^{-3}	0.250	8.2×10^{-3}	0.123	2.6×10^{-4}
0.146	1.4×10^{-4}	0.326	4.1×10^{-2}	0.125	1.1×10^{-3}
0.169	5.8×10^{-5}	0.335	7.1×10^{-2}	0.146	1.4×10^{-4}
0.208	2.7×10^{-4}	0.368	3.3×10^{-2}	0.169	5.9×10^{-5}
0.326	1.2×10^{-4}	0.375	1.5×10^{-2}	0.208	2.7×10^{-4}
0.335	1.9×10^{-4}	0.376	2.3×10^{-2}	0.326	1.2×10^{-4}
0.368	8.0×10^{-5}	0.478	5.5×10^{-1}	0.335	1.9×10^{-4}
0.376	5.5×10^{-5}	0.619	1.5×10^{-2}	0.368	8.0×10^{-5}
0.478	1.1×10^{-3}	0.648	3.8×10^{-2}	0.376	5.5×10^{-5}
0.619	2.6×10^{-5}	0.662	9.4×10^{-2}	0.619	2.6×10^{-5}
0.662	1.6×10^{-4}	0.722	5.3×10^{-2}	0.662	1.6×10^{-4}
0.722	8.8×10^{-5}	0.756	8.2×10^{-3}	0.722	8.8×10^{-5}

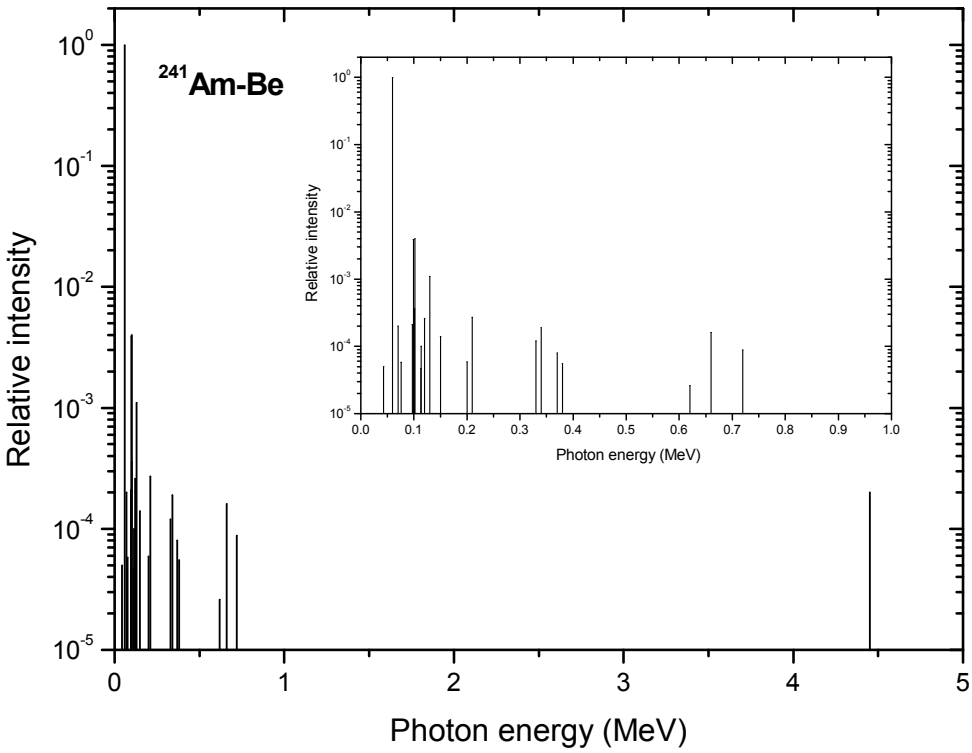

Figure 13. Plot of gamma ray lines from an ^{241}Am-Be source. The insert shows the energy region up to 1 MeV. Note the logarithmic Y-axes. Intensities are normalised to a total intensity of 1.0

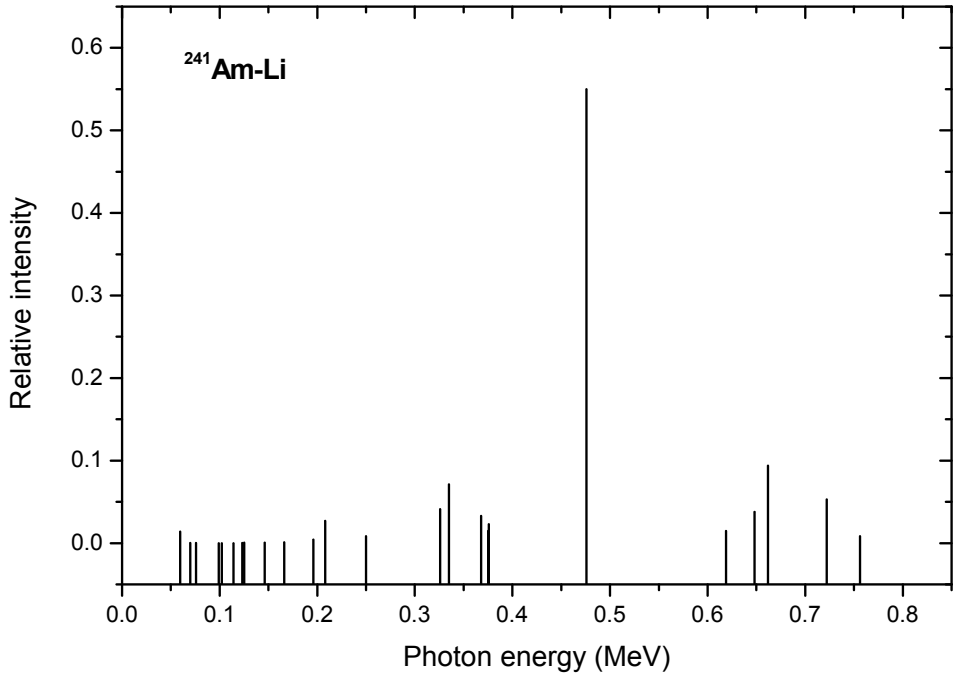

Figure 14. Plot of gamma ray lines from an ^{241}Am-Li source with lead shielding. Intensities are normalised to a total intensity of 1.0

Appendix B: ^{252}Cf and D_2O moderated ^{252}Cf source photon spectra

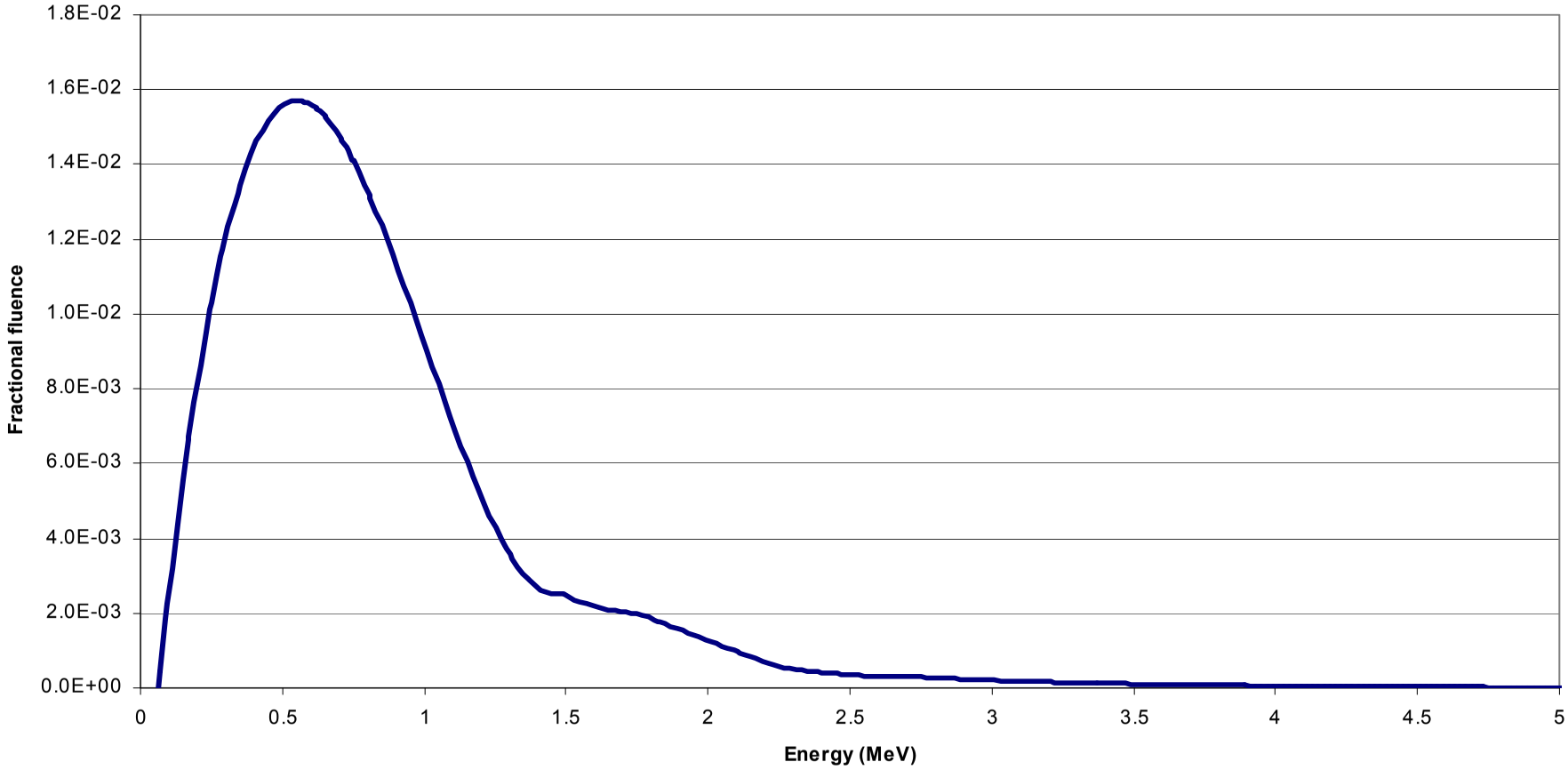

Figure 15. Estimated fractional photon fluence spectrum of the NPL ^{252}Cf neutron source. The curve is interpolated from data provided in ICRU 26.

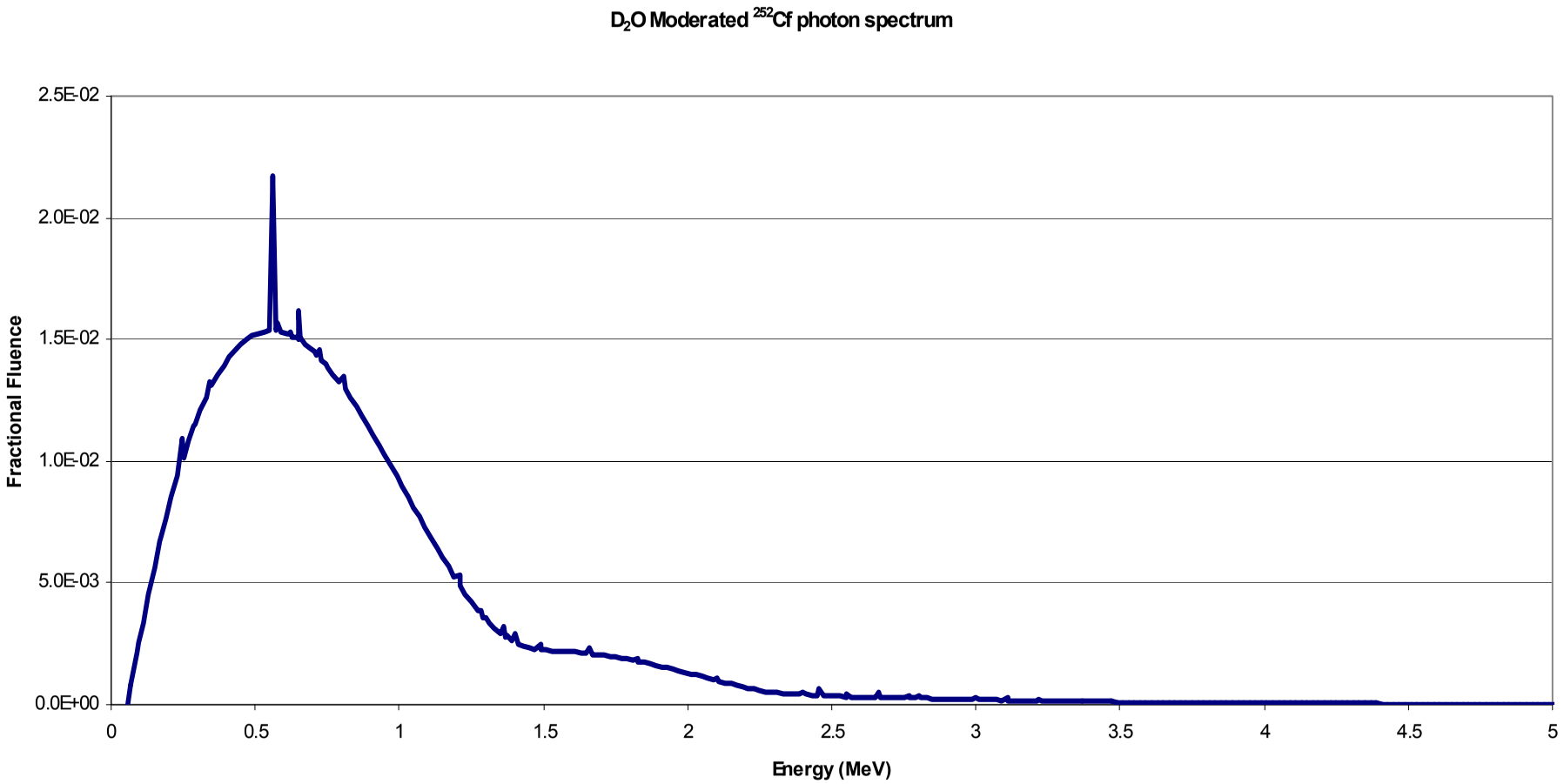

Figure 16. Estimated fractional fluence photon spectrum of NPL D_2O moderated ^{252}Cf neutron source. The smooth curve is a result of the ^{252}Cf decay and the sharp peaks are the result of radiative neutron capture by the cadmium sheath.

Appendix C: Photon response of Geiger-Müller detectors

Table 11. Tabulated relative response of Geiger-Müller detectors

Source	Photon energy (keV)	Response relative to ^{60}Co							
		MX164A	Rel. Error	MX164B	Rel. Error	ZP1100	Rel. Error	MX163	Rel. Error
Start Point	20	0.00	-	0.00	-	0.00	-	0.00	-
40-kV x ray	33	0.55	1.2%	0.40	3.2%	0.58	3.2%	0.38	3.2%
^{241}Am	59.5	0.82	1.9%	1.01	3.2%	1.05	3.2%	0.86	3.2%
60-kV x ray	48	0.95	1.2%	1.16	1.2%	1.44	1.2%	1.22	1.2%
80-kV x ray	65	0.95	1.4%	0.72	3.3%	1.07	3.2%	0.91	3.2%
100-kV x ray	83	0.66	1.1%	0.49	3.2%	0.64	3.2%	0.67	3.3%
120-kV x ray	100	1.03	1.2%	0.73	3.2%	1.00	3.2%	0.93	3.3%
150-kV x ray	118	1.15	4.8%	1.02	3.2%	1.49	3.2%	1.30	3.3%
20-kV x ray	164	1.01	1.9%	0.62	3.1%	0.91	3.2%	0.96	3.3%
250-kV x ray	208	0.92	1.1%	0.41	8.3%	0.69	8.3%	0.66	8.5%
300-kV x ray	250	0.78	1.4%	0.52	3.3%	0.86	3.1%	1.07	3.2%
^{137}Cs	661	0.94	1.2%	0.94	1.2%	0.99	1.4%	1.11	1.0%
^{60}Co	1250	1.00	0.0%	1.00	1.2%	1.00	0.0%	1.00	0.0%
Hinkley	6000	1.26	-	1.26	-	-	-	1.40	-
	10000	-	-	-	-	1.37	-	-	-

Appendix D: A new set of Geiger-Müller detectors

The age, past performance, and evidence of alteration to the Geiger tubes used in these experiments means that their reliability in the future cannot be guaranteed. As part of this project a new set of Geiger tubes was procured and a new electronic set-up using the more maintainable NIM electronics was researched.

The following energy-compensated halogen-quenched Geiger-Müller detectors, manufactured by Centronic, were purchased and mounted in custom designed stands;

- One ZP1201
- One ZP1301
- Three ZP1321s

The ZP1201 detector is the most sensitive tube and is more sensitive than any of the tubes used in this study. The addition of this detector allows the dose rate that can reliably be measured, to be lowered to 10^{-3} mGy/hr. Multiple ZP1321s were purchased to provide redundancy and to reduce the risk of equipment failure leading to a loss of capability. The ZP1301 was purchased to provide the capability of performing measurements in higher intensity photon fields, up to 1×10^{4} mGy/h should the need arise. This set of detectors provides a redundancy in numbers and design and so reduces the possibility of systematic errors.

The detector mountings were designed to minimise the distortion of the detector photon response and to limit the detector neutron response. The aluminium mounts contain the anode resistor and allow connection to the detector via a BNC connector. The anode resistance values used were those recommended by Centronic and are shown in the table below along with other information about the detectors.

Various systems of electronics were tested, but the most suitable and flexible system that could integrate with current data acquisition systems was found to be a NIM based system. This allows most of the electronics to be situated remotely from the detectors and allows the use of current computer based data acquisition software.

The appropriate high voltage is supplied via a SHV cable to the potential divider, which in turn supplies the GM tube. Anode signals are fed into an ORTEC 113 voltage sensitive preamplifier by means of the potential divider. This allows the signal to be transmitted across the 50m cables from the low-scatter area to the control room. The signal is input into a width/delay unit to allow control of the dead-time at relatively low count rates and then into the computer-controlled scaler.

Initial measurements indicate a good agreement of the detector response with the measurements with the old system. It is recommended that, following assurance and verification of the detector characteristics, this new system should be used for future measurements.

Detector	Operating voltage (V)	Anode resistor	Dead-time (using described set-up)
ZP1201	500	10 GΩ	120 μs
ZP1301	575	2.2 GΩ	30 μs
ZP1321	575	4.7 GΩ	60 μs

6 REFERENCES

1 International Organisation for Standardization, *Reference neutron radiations- Part 1: Characteristics and methods of production*, International Standard ISO 8529-1 (Geneva, Switzerland, ISO) (2001).

2 J.C. McDonald, R.V. Griffith, P.A. Plato and A. Miklos, *Measurement of Gamma Ray Dose from a Moderated ^{252}Cf Source*, Radiat. Prot. Dosim. **9**, No. 2, 113-118 (1984).

3 F. Spurný, I. Votockova, J.-F Bottollier-Depois, J. Kurkdjian and D. Paul, *Test of Instruments for Neutron and Gamma Ray Measurements at Several Radionuclide Neutron Sources*, Radiat, Prot. Dosim. **70**, No. 1-4, 353-356 (1997).

4 K. Józefowicz, N. Golnik and M. Zielczyński, *Standard fields of old neutron sources-parameters and traceability,* Radiat, Prot. Dosim. **110**, No. 1-4, 107-110 (2004).

5 F. Langner, S. Löb, R. Nolte, V. Gressier, B. Asselineau, V. Lacoste and L. Lebreton, *Photon Contributions to Ambient Dose Equivalent H*(10) in the Wide-Spectrum Neutron Reference Fields of the IRSN,* Radiat, Prot. Dosim. **126**, No. 1-4, 145-150 (2007).

6 International Commission on Radiation Units and Measurements, *Neutron Dosimetry for Biology and Medicine,* ICRU Report 26 (ICRU, Bethesda, MD) (1977).

7 *Wide range gamma radiation monitoring instrument,* United Kingdom Atomic Energy Authority, AEA Winfrith, (1973).

8 *Geiger-Muller Tube ZP1100- development sample data*, Mullard (1975).

9 *MicroShield 7.00*, Grove Software Inc, (2005), http://www.radiationsoftware.com/.

10 J.G. Owen, D.R. Weaver and J. Walker, *Neutron Spectra from Am/F and Am/Li(α,n) Sources.* International Conference on Nuclear Data for Science and Technology, Antwerp 6 - 10 September (1982).

11 H. Tagziria, Private communication. NPL, (1994).

12 H. Tagziria, N.J. Roberts, and D.J. Thomas, *Measurements of the ^{241}Am-Li radionuclide neutron source spectrum*, Nucl. Instrum and Meth. **A 510** 346-356 (2003).

13 R.B. Schwartz and C.M. Eisenhauer, *The Design and Construction of D_2O-Moderated ^{252}Cf Source for calibrating Neutron Personal Dosemeters Used at Nuclear Power Reactors*, NUREG/CR-1204 (1980).

14 Evaluated Nuclear Structure Data Files (ENSDF), National Nuclear Data Center, Brookhaven, (http://www.nndc.bnl.gov/ensdf/).

15 A.A Mowlavi and R. Koohi-Fayegh, *Determination of 4.438 MeV γ-ray to neutron emission ratio from a ^{241}Am-^{9}B neutron source,* App. Rad. & Isotopes **60,** 959-962 (2004).

16 E.W. Lees and D. Lindley, *Characteristic gamma-ray spectra from light elements in $^{241}Am(\alpha,n)$ sources and their use in detecting impurities,* Report by the Nuclear Physics Division, AERE Harwell, Oxfordshire, 1977 AERE-R 8891.

17 Japan Atomic Energy Agency, Nuclear Data Center, JENDL Data, B(α,n) cross-section files (http:/wwwndc.jaea.go.jp/index.html).

18 Evaluated Nuclear Data Files (ENDF), National Nuclear Data Center, Brookhaven, (http://www.nndc.bnl.gov/exfor/endf00.htm).

19 Database of prompt gamma rays from slow neutron capture for elemental analysis, International Atomic Energy Agency, Vienna, 2006. ISBN 92–0–101306–X.

20 D.T.L. Jones and W.R. McMurray, *The Neutron sensitivity of a Geiger-Müller Counter between 0.5 and 8 MeV*, Health Physics **45**, No. 3, 659-663 (1983).

21 D.T.L. Jones, C.M. Bartle, J.H. Hough and W.E. McMurray, *Absolute measurement of the Neutron sensitivity of a ZP1320 Geiger-Müller counter using the associated particle technique*, Health Physics **43**, No. 5, 715-718 (1982).

22 V.E. Lewis and J.B. Hunt, *Fast Neutron Sensitivities of Geiger-Mueller Counter gamma Dosemeters*, Phys. Med. Biol., **23**, No. 5, 999-893 (1978).

23 V.E. Lewis and D.J. Young, *Measurement of the fast neutron sensitivities of Geiger-Mueller counter gamma dosemeters,* Phys. Med. Biol., **22**, No. 3**,** 476-480 (1977).

24 S. Guldbakke, R. Jahr, H. Lesiecki and H. Scholermann, *Neutron response of Geiger-Müller photon dosemeters for neutron energies between 100 keV and 19 MeV*, Health Physics, **39**, 963-969 (1980).

25 J.H. Hough, *A modified lead attenuation method to determine the fast neutron sensitivity k_u of a photon dosemeter*, Phys. Med. Biol., **24**, No. 4, 737-747 (1979).

26 S. Croft and D.R. Weaver, *The Measurement of the Gamma-ray field Accompanying Neutron Beams from a Particle Accelerator by Means of a Geiger-Müller Counter,* Nucl. Instrum and Meth. **A 276,** 614-621 (1989).

27 *Radiation Detection and Measurement,* 3rd edition, Glenn F. Knoll, Wiley, 2000 Chapt. 4, P 119.

28 R.F. Angliss, C.J. Moretti, R.F. Nutbrown, *Proposed specification for a primary standard of air kerma for ^{60}Co, ^{137}Cs and ^{192}Ir γ-ray sources,* NPL Report CIRM 53, September 2001

29 International Organisation for Standardization, *X and gamma reference radiation for calibrating dosemeters and doserate meters and for determining their response as a function of photon energy - Part 1: Radiation characteristics and production methods*, International Standard ISO 4037-1 (Geneva, Switzerland, ISO) (1996).

30 Private communication, P. Burgess, NPL (2007).

31 International Commission on Radiological Protection, *Conversion Coefficients for use in Radiological Protection against External radiation,* Annals of the ICRP Publication 74, Pergamon (1996).

32 International Commission on Radiation Units and Measurements, *Conversion Coefficients for use in Radiological Protection against External radiation,* ICRU Report 57 (ICRU, Bethesda, MD) (1998).

33 International Commission on Radiation Units and Measurements, *Tissue Substitutes in Radiation Dosimetry and Measurement,* ICRU Report 44 (ICRU, Bethesda, MD) (1989).

34 International Commission on Radiation Units and Measurements, *Nuclear Data for Neutrons and Proton Radiotherapy and for Radiation Protection,* ICRU Report 63(ICRU, Bethesda, MD) (2000).

35 International Organisation for Standardization, *Reference neutron radiations – Part 2; calibration fundamentals of radiation protection devices related to the basic quantities characterizing the radiation field*, International Standard ISO 8529-2, (Geneva, Switzerland, ISO) (2000).

36 J.C. McDonald, R.B. Schwartz and R.H. Thomas, *Neutron Dose equivalent Conversion Coefficients have changed in the last Forty Years . . .Haven't they?,* Radiat. Prot. Dosim. **78**, No. 2, 147-149 (1998).